Advanced Modeling and Simulation in Engineering Sciences

RESEARCH ARTICLE

Open Access

CrossMark

Isogeometric analysis-based reduced order modelling for incompressible linear viscous flows in parametrized shapes

Filippo Salmoiraghi, Francesco Ballarin, Luca Heltai and Gianluigi Rozza[*]

[*]Correspondence:
gianluigi.rozza@sissa.it
mathLab, Mathematical Analysis,
Modelling and Applications,
Mathematics Area, SISSA
International School for
Advanced Studies, Via Bonomea
265, 34136 Trieste, Italy

Abstract

In this work we provide a combination of isogeometric analysis with reduced order modelling techniques, based on proper orthogonal decomposition, to guarantee computational reduction for the numerical model, and with free-form deformation, for versatile geometrical parametrization. We apply it to computational fluid dynamics problems considering a Stokes flow model. The proposed reduced order model combines efficient shape deformation and accurate and stable velocity and pressure approximation for incompressible viscous flows, computed with a reduced order method. Efficient offline–online computational decomposition is guaranteed in view of repetitive calculations for parametric design and optimization problems. Numerical test cases show the efficiency and accuracy of the proposed reduced order model.

Keywords: Isogeometric analysis (IGA), Reduced order models (ROM), Proper orthogonal decomposition (POD), Stokes flows, Free form deformation (FFD), Computational fluid dynamics (CFD)

Focus and motivation

The capability to perform fast simulations is becoming increasingly relevant for several applications in engineering sciences, related for instance to naval and aeronautical engineering, as well as biomedicine. To this end, reduced basis methods [1,2], proper orthogonal decomposition [3–5], proper generalized decomposition [6,7], hierarchical model reduction [8–10], or more in general reduced order modelling (ROM) techniques [11], have received considerable attention in the last decades. ROMs do not replace, but rather build upon as an add-on, high-fidelity methods such as finite element, finite volume or discontinuous Galerkin methods. Indeed, the choice of the high-fidelity solver can be made depending on the particular problem at hand and on pre-existing expertise and software availability. Current literature has explored a broad variety of options, including reduced order models based on a finite element high-fidelity discretization (e.g. [2,12–15]), finite volume (e.g. [16–19]) and finite difference methods (e.g. [20–22]). More recently, investigations towards the coupling with discontinuous Galerkin methods for multiscale problems [23] or domain-decomposition approaches [24–26], spectral element methods [27,28], and extended finite element methods [29,30] have been carried out.

Springer Open

Salmoiraghi *et al. Adv. Model. and Simul. in Eng. Sci.*(2016)3:21

Page 2 of 22

The aim of this work is to embed *isogeometric analysis* (IGA) [31,32] as a high-fidelity discretization option in a ROM setting, for the simulation of incompressible linear viscous flows [33–36] and to propose a complete workflow (pipeline) integrated with free from deformation (FFD) as efficient geometrical parametrisation. The latter is enhanced into an IGA context ready to be used within reduced order method (POD). A considerable advantage of IGA with respect to classical finite element analysis is the possibility to avoid any geometrical approximation error and to perform direct design-to-analysis simulations by replacing classical mesh generation, and employing the same class of functions used for geometry parameterization in CAD packages during the analysis process. Even though most modern CAD tools are based on boundary representation (B-Rep) objects, it is still possible to use them in three-dimensional isogeometric analysis, by extending the computational domain inside (or outside) the enclosing (or enclosed) CAD surface (see, for example, [37]). A robust and reliable solution for such passage is still lacking, making this step an open question. However, the superior approximation properties of IGA methods make their adoption appealing also in biomedical and bioengineering applications [38], notwithstanding the fact that in this case the geometry is normally obtained through an approximate NURBS reconstruction of medical images.

Once the three-dimensional tensor product representation of the geometry is available, there is no distinction in computational cost or implementation complexity, with respect to simulations done on elementary geometries.

Preliminary related IGA-ROMs have been applied to steady potential flows [39,40], parabolic problems [41] or shell structural models [42]. In this work offline−online IGA-ROM is applied for the development of stable computational reduction strategies for viscous flows problems in parametrized shapes by FFD means. We investigate IGA-ROMs in a different context with respect to earlier works [39,40]. In [40] the authors neglect viscous terms and formulate the high-fidelity discretization in terms of boundary integral equations and boundary element methods (BEM) to study external flows. The main novelty of the present work, besides the investigation of the other side of the spectrum of incompressible regimes (that is, when the Reynolds number tends to zero), is the coupling of FFD techniques applied to IGA geometries, for internal flows, and using finite element based IGA, in view of studies dealing with nonlinear viscous flows, for which BEM is not suited.

We would like to remark here that, although the background idea is the same as the one presented in [40], several technical issues are fundamentally different. One of the most obvious one is that the discrete systems obtained through boundary integral formulations are in general full, which implies that higher order and higher continuity finite element spaces do not influence the bandwidth of the resulting matrix. In finite element formulations of IGA methods, however, this is an important issue, and it may result in reduced performances also of the final reduced order model. In this work we show how the increased bandwidth of the high fidelity solver does not influence negatively on the combination IGA-ROM, provided that stable approximations are used for the high fidelity solver.

The proposed integrated approach is composed of the following numerical techniques: (i) *isogeometric analysis*, that integrates the geometrical representation of the domain and the finite dimensional approximation of the fluid dynamics problem [32], (ii) *free-form deformation* to efficiently deform the computational domain by means of few geometrical

Salmoiraghi *et al. Adv. Model. and Simul. in Eng. Sci.* (2016) 3:21

Page 3 of 22

parameters [43], and (iii) *proper orthogonal decomposition*-based reduced order modelling to generate a stable reduced basis to be queried to cut down the computational cost of numerical simulations [44]. This integration has been introduced in a preliminary version in [45].

The approach we present is completely integrated and automatic from CAD to simulation, taking advantage of IGA and FFD perspectives for the accurate and efficient management of parametrized domains and shapes. The split between offline and online computational steps is crucial and it allows the versatility of bringing this proposed computational approach on very different devices, scenarios and situations in design and optimization, for instance.

The structure of the work is as follows. The parametrized formulation and the IGA method are introduced in "Problem formulation and isogeometric analysis-based high-fidelity approximation" section; necessary assumptions related to the offline–online decomposition are also summarized. "Shape parametrization by free-form deformation" section summarizes the free-form deformation map which is employed to prescribe geometrical variations. The proposed stable POD–Galerkin ROM is introduced in "A POD-Galerkin ROM for parametrized Stokes equations" section, and 2D and 3D numerical tests are performed in "Numerical results" section into an optimisation framework. Finally, conclusions and perspectives follow in "Conclusions and future work" section.

Problem formulation and isogeometric analysis-based high-fidelity approximation

Parametrized formulation

The problem of interest throughout this work is a parametrized incompressible steady Stokes problem, obtained as a simplification of Navier–Stokes equations when inertial forces can be neglected, compared to viscous forces. Parameters of interest, denoted by $\boldsymbol{\mu} \in \mathcal{D} \subset \mathbb{R}^G$, are related to the geometrical representation of the domain $\Omega = \Omega(\boldsymbol{\mu}) \subset \mathbb{R}^d$. The parametrized Stokes problem reads: find $(\boldsymbol{u}(\boldsymbol{\mu}), p(\boldsymbol{\mu}))$ such that

$$\begin{cases} -\nu \Delta \boldsymbol{u}(\boldsymbol{\mu}) + \nabla p(\boldsymbol{\mu}) = \boldsymbol{f}(\boldsymbol{\mu}), & \text{in } \Omega(\boldsymbol{\mu}), \\ \nabla \cdot \boldsymbol{u}(\boldsymbol{\mu}) = 0, & \text{in } \Omega(\boldsymbol{\mu}), \end{cases} \tag{1}$$

with boundary conditions

$$\begin{cases} \boldsymbol{u}(\boldsymbol{\mu}) = \boldsymbol{g}, & \text{on } \Gamma_D \neq \emptyset, \\ \boldsymbol{u}(\boldsymbol{\mu}) = \boldsymbol{0}, & \text{on } \Gamma_W(\boldsymbol{\mu}), \\ \nu \nabla \boldsymbol{u}(\boldsymbol{\mu}) \cdot \boldsymbol{n} - p(\boldsymbol{\mu})\boldsymbol{n} = \boldsymbol{h}, & \text{on } \Gamma_N \neq \emptyset, \end{cases} \tag{2}$$

representing *essential* and *natural* boundary conditions for Stokes equations, respectively. Here ν is a constant kinematic viscosity, while $\boldsymbol{f}(\boldsymbol{\mu})$, $\boldsymbol{g}$ and $\boldsymbol{h}$ are prescribed forcing terms, boundary velocity profiles, and boundary tractions, respectively. For simplicity we assume that the sections Γ_D and Γ_N do not depend on the geometrical parameters, while the remaining part of the boundary $\Gamma_W(\boldsymbol{\mu}) = \partial\Omega(\boldsymbol{\mu}) \setminus (\Gamma_D \cup \Gamma_N)$ may depend on $\boldsymbol{\mu}$.

Isogeometric formulations of Stokes flows have been extensively studied in the literature. We refer to [46] for a comprehensive analysis of stable choices of isogeometric finite element spaces, and to [47] for an alternative formulation based on boundary integral equations.

Salmoiraghi *et al. Adv. Model. and Simul. in Eng. Sci.* (2016) 3:21

Page 4 of 22

Isogeometric description of the parametrized domain

A CAD representation of the domain is usually obtained through a set of control points $\{\boldsymbol{P}_i\}_{i=1}^{\mathcal{N}_g}$, where in general $\boldsymbol{P}_i \in \mathbb{R}^d$ is a d-dimensional *IGA control point*,[1] whose position depends on the geometrical parameters $\boldsymbol{\mu}$.

A d-dimensional geometrical representation is obtained by tensor product of d one-dimensional *B-spline basis functions*, denoted by $\left\{\xi_i^d(s)\right\}_{i=1}^{\mathcal{N}_d}$, $\xi_i^d : [0, 1] \to \mathbb{R}$, and defined recursively as

$$\xi_{i,k}^d(s) = \frac{s - \theta_i^d}{\theta_{i+k}^d - \theta_i^d}\xi_{i,k-1}^d(s) + \frac{\theta_{i+k+1}^d - s}{\theta_{i+k+1}^d - \theta_{i+1}^d}\xi_{i+1,k-1}^d(s) \quad k = 1, \ldots, p_d, \tag{3}$$

where

$$\xi_{i,0}^d(s) = \begin{cases} 1, & \theta_i^d \leq s \leq \theta_{i+1}^d, \\ 0, & \text{otherwise}. \end{cases}$$

and $\xi_i^d(s) := \xi_{i,p_d}^d(s)$. Here $\boldsymbol{\theta^d} = \{\theta_1^d, \theta_2^d, \ldots, \theta_{n+p+1}^d\}^T$, $\theta_i^d \in \mathbb{R}$, is the d-th *knot vector*, a non-decreasing set of coordinates in the s parameter space, whereas p_d is the polynomial order of the basis functions along the direction d.

Multivariate B-spline basis functions in $\mathbb{R}^d$ (see for example Fig. 1) can then be defined by tensor product as

$$B_i(\boldsymbol{s}) = \xi_{i_1}^1(s_1) \ldots \xi_{i_d}^d(s_d), \qquad i_k = 1 \ldots \mathcal{N}_{g,k}, \qquad i = 1 \ldots \mathcal{N}_g := \prod_{k=1}^d \mathcal{N}_{g,k}.$$

For simplicity of exposition we work on single patch geometries, where the reference domain is $[0, 1]^d$, and we refer to [32,48] and the references therein for possible generalizations to multipatch geometries.

The reference domain $\overline{\Omega} = [0, 1]^d$ can be deformed into the computational (parametrized) domain $\Omega(\boldsymbol{\mu})$, by introducing a parametrized map $\boldsymbol{c}(\cdot; \boldsymbol{\mu}) : \overline{\Omega} \to \mathbb{R}^d$:
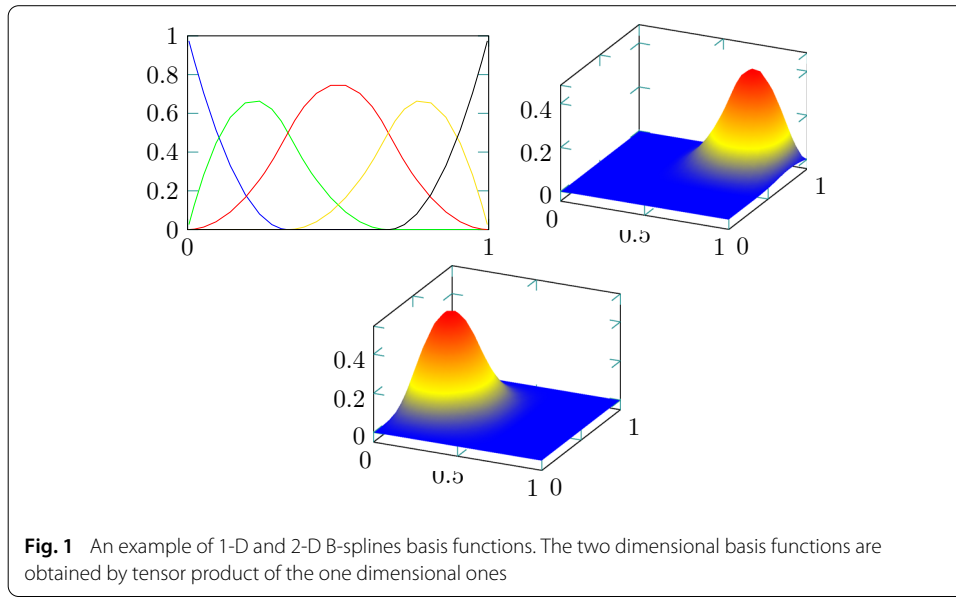
$$\boldsymbol{c}(\boldsymbol{s}; \boldsymbol{\mu}) := \sum_{i=1}^{\mathcal{N}_g} B_i(\boldsymbol{s})\boldsymbol{P}_i(\boldsymbol{\mu}), \qquad \Omega(\boldsymbol{\mu}) = \boldsymbol{c}(\overline{\Omega}; \boldsymbol{\mu}), \tag{4}$$

that depends on the parameter vector $\boldsymbol{\mu}$ through the set of $\mathcal{N}_g$ IGA control points $\{\boldsymbol{P}_i\}_{i=1}^{\mathcal{N}_g}$, where the subscript g indicates *geometry*. Different parameter values will produce different IGA control points and, thus, different computational domains. We will characterize in "Shape parametrization by free-form deformation" section how to efficiently prescribe the dependence of $\boldsymbol{P}_i$ on $\boldsymbol{\mu}$ to obtain a broad range of admissible shapes. This parametrization is crucial to embed IGA in a ROM setting dealing with parametric shapes.

Weak formulation on the reference domain and discrete problem

In order to derive a discrete approximation of the parametrized Stokes problem (1)–(2), we introduce a weak formulation on the reference domain $\overline{\Omega}$. For simplicity of exposition, we will use the same notation we used in Eq. (1) for the velocity and pressure fields, even though here the domain is different. Denote by $V = [H^1(\overline{\Omega})]^d$ and $Q = L^2(\overline{\Omega})$ the velocity and pressure spaces. Multiplying (1) by test functions $\boldsymbol{v} \circ \mathbf{c}$ and $q \circ \mathbf{c}$ (for the velocity and

---

[1]In the next section we will introduce another set of control points, related to the free-form deformation, which will be denoted FFD control points.

Salmoiraghi *et al. Adv. Model. and Simul. in Eng. Sci.*(2016)3:21

Page 5 of 22

Fig. 1 An example of 1-D and 2-D B-splines basis functions. The two dimensional basis functions are obtained by tensor product of the one dimensional ones

pressure field, respectively), integrating by parts and pulling back to the reference domain, we obtain the following problem: given $\boldsymbol{\mu} \in \mathcal{D}$, find $\boldsymbol{u} \in V$ and $p \in Q$ such that

$$\begin{cases} a(\boldsymbol{u}, \boldsymbol{v}; \boldsymbol{\mu}) + b(p, \boldsymbol{v}; \boldsymbol{\mu}) = F(\boldsymbol{v}; \boldsymbol{\mu}), & \forall \boldsymbol{v} \in V, \\ b(q, \boldsymbol{u}; \boldsymbol{\mu}) = 0, & \forall q \in Q, \end{cases} \tag{5}$$

where the bilinear forms appearing in (5) are:

$$a(\boldsymbol{u}, \boldsymbol{v}; \boldsymbol{\mu}) := \int_{\overline{\Omega}} \nabla \boldsymbol{u} \, \boldsymbol{J}^{-1}(\boldsymbol{\mu}) \boldsymbol{J}^{-T}(\boldsymbol{\mu}) \det(\boldsymbol{J}(\boldsymbol{\mu})) : \nabla \boldsymbol{v} \, \mathrm{d}\boldsymbol{s}, \quad \forall \boldsymbol{u}, \boldsymbol{v} \in V,$$

$$b(p, \boldsymbol{v}; \boldsymbol{\mu}) := - \int_{\overline{\Omega}} p \, \mathrm{tr}(\boldsymbol{J}^{-1}(\boldsymbol{\mu}) \det(\boldsymbol{J}(\boldsymbol{\mu})) \nabla \boldsymbol{v}) \, \mathrm{d}\boldsymbol{s}, \quad \forall \boldsymbol{v} \in V, p \in Q.$$

Here, $\boldsymbol{J}(\boldsymbol{\mu})$ is the Jacobian of the mapping $\boldsymbol{c}(\boldsymbol{s}; \boldsymbol{\mu})$. The linear form $F(\boldsymbol{v}; \boldsymbol{\mu})$ encodes forcing terms, essential boundary conditions (by divergence-free lifting) and natural boundary conditions.

Isogeometric approximations of Stokes flows (see, for example [46]) violate somehow the *isogeometric paradigm*, in the sense that we require two different B-spline spaces for the velocity and pressure fields in order to satisfy the *inf-sup* condition, and only one of the two is usually taken to be the same as the geometrical B-spline space. We introduce $V^{\mathcal{N}} \subset V$ and $Q^{\mathcal{N}} \subset Q$, of dimensions $\mathcal{N}_u$ and $\mathcal{N}_p$ respectively. To differentiate w.r.t. to the geometric basis functions (which are always taken to be scalar, since we encode the dimensional information in the control points), we use the following, more general, notation

$$\boldsymbol{u}(\boldsymbol{s}) \approx \boldsymbol{u}^{\mathcal{N}}(\boldsymbol{s}) = \sum_{i=1}^{\mathcal{N}_u} \phi_i(\boldsymbol{s}) u_i, \quad p(\boldsymbol{s}) \approx p^{\mathcal{N}}(\boldsymbol{s}) = \sum_{i=1}^{\mathcal{N}_p} \varphi_i(\boldsymbol{s}) p_i, \tag{6}$$

to indicate objects of $V^{\mathcal{N}} \subset V$ and $Q^{\mathcal{N}} \subset Q$, where

$$V^{\mathcal{N}} = \mathrm{span}\{\phi_i, i = 1, \ldots, \mathcal{N}_u\} \quad \text{and} \quad Q^{\mathcal{N}} = \mathrm{span}\{\varphi_i, i = 1, \ldots, \mathcal{N}_p\}, \tag{7}$$

respectively. An alternative notation, that allows one to distinguish between the properties of the different isogeometric spaces (see, for example, [36,46]) is given by the following:

$$V^{\mathcal{N}} \equiv \mathcal{S}_{\alpha_1,\ldots,\alpha_d}^{p_1,\ldots,p_d} := \mathrm{span}\{\phi_i\}_{i=1}^{\mathcal{N}_u}, \qquad Q^{\mathcal{N}} \equiv \mathcal{S}_{\alpha_1,\ldots,\alpha_d}^{p_1,\ldots,p_d} := \mathrm{span}\{\varphi_i\}_{i=1}^{\mathcal{N}_p}, \tag{8}$$

Salmoiraghi *et al. Adv. Model. and Simul. in Eng. Sci.*(2016)3:21

Page 6 of 22

where p_i and α_i represent respectively the degree and the maximal regularity in the ith direction.

If one chooses to use the same basis functions for the geometry and the velocity (for example), then ϕ_i are vector versions of B_i, and $\mathcal{N}_u = d\mathcal{N}_g$, where $\mathcal{N}_g$ is the number of the geometry basis functions. For an extensive discussion on the choices of stable pairs of isogeometric finite element approximations of Stokes flows, we refer the reader to [46] and the references therein. In this work we used a Taylor-Hood approximation (as presented, for example, in [36]), in which the pressure space is taken to be one degree less of the velocity space, *maintaining the same knot vectors* of the geometry and velocity spaces, i.e., we consider pairs of spaces given by $(\mathcal{S}^{p,\dots,p}_{p-1,\dots,p-1} - \mathcal{S}^{p-1,\dots,p-1}_{p-2,\dots,p-2})$ which satisfy the inf-sup condition and represent a good balance between attainable accuracy and computational efficiency.

The isogeometric Galerkin formulation of the problem becomes: given $\boldsymbol{\mu} \in \mathcal{D}$, find $\boldsymbol{u}^{\mathcal{N}} \in V^{\mathcal{N}}$ and $p^{\mathcal{N}} \in Q^{\mathcal{N}}$ such that

$$\begin{cases} a(\boldsymbol{u}^{\mathcal{N}}, \boldsymbol{v}^{\mathcal{N}}; \boldsymbol{\mu}) + b(p^{\mathcal{N}}, \boldsymbol{v}^{\mathcal{N}}; \boldsymbol{\mu}) = F(\boldsymbol{v}^{\mathcal{N}}; \boldsymbol{\mu}) & \forall \boldsymbol{v}^{\mathcal{N}} \in V^{\mathcal{N}} \\ b(q^{\mathcal{N}}, \boldsymbol{u}^{\mathcal{N}}; \boldsymbol{\mu}) = 0 & \forall q^{\mathcal{N}} \in Q^{\mathcal{N}} \end{cases} \tag{9}$$

where $\boldsymbol{u}^{\mathcal{N}} = \boldsymbol{u}^{\mathcal{N}}(\boldsymbol{\mu}) \in V^{\mathcal{N}}$ and $p^{\mathcal{N}} = p^{\mathcal{N}}(\boldsymbol{\mu}) \in Q^{\mathcal{N}}$ denote the high-fidelity velocity and pressure solutions, respectively. Equation (9) can be written in matrix form as

$$\begin{bmatrix} \underline{\mathbf{K}}(\boldsymbol{\mu}) & \underline{\mathbf{B}}^T(\boldsymbol{\mu}) \\ \underline{\mathbf{B}}(\boldsymbol{\mu}) & \mathbf{0} \end{bmatrix} \begin{Bmatrix} \underline{\mathbf{u}}(\boldsymbol{\mu}) \\ \underline{\mathbf{p}}(\boldsymbol{\mu}) \end{Bmatrix} = \begin{Bmatrix} \underline{\mathbf{f}}(\boldsymbol{\mu}) \\ \mathbf{0} \end{Bmatrix}, \tag{10}$$

where

$$\underline{\mathbf{K}}_{ij}(\boldsymbol{\mu}) = a(\phi_j, \phi_i; \boldsymbol{\mu}), \qquad \underline{\mathbf{B}}_{ij}(\boldsymbol{\mu}) = b(\varphi_i, \phi_j; \boldsymbol{\mu}), \qquad \underline{\mathbf{f}}_i(\boldsymbol{\mu}) = F(\phi_i; \boldsymbol{\mu}), \tag{11}$$

and we indicate with $\underline{\mathbf{u}}(\boldsymbol{\mu})$ and $\underline{\mathbf{p}}(\boldsymbol{\mu})$ the $\mathbb{R}^{\mathcal{N}_u}$ and $\mathbb{R}^{\mathcal{N}_p}$ vector of coefficients of the discrete, high-fidelity, velocity and pressure fields respectively.

Affine parametric dependence assumption

In this work we seek for an offline–online decomposition of the computational stages, as required in the reduced order modelling context for an efficient evaluation of the ROM [1]. During the offline stage, which we will summarize in "Reduced basis construction through proper orthogonal decomposition" section, we carry out all expensive computations (related to the IGA high-fidelity model); in contrast, we look for an online phase (related to the ROM) which is extremely fast (see "Reduced order approximation through Galerkin projection on the reduced spaces" section). In order to achieve this, we require that matrices and vectors in (11) fullfil the following affine parametric dependence assumption:

$$\underline{\mathbf{K}}(\boldsymbol{\mu}) = \sum_{q=1}^{Q_K} \Theta_q^K(\boldsymbol{\mu}) \underline{\mathbf{K}}^q, \qquad \underline{\mathbf{B}}(\boldsymbol{\mu}) = \sum_{q=1}^{Q_B} \Theta_q^B(\boldsymbol{\mu}) \underline{\mathbf{B}}^q, \qquad \underline{\mathbf{f}}(\boldsymbol{\mu}) = \sum_{q=1}^{Q_f} \Theta_q^f(\boldsymbol{\mu}) \underline{\mathbf{f}}^q. \tag{12}$$

We employ the empirical interpolation method (EIM) [49] to approximate this assumption up to a desired tolerance. See also [50–53] for the application of EIM to viscous flows in parametrized domains.

Shape parametrization by free-form deformation

In this section we show how to relate geometrical parameters $\boldsymbol{\mu}$ to the IGA control points position $\boldsymbol{P}_i(\boldsymbol{\mu})$. Unfortunately, choosing the IGA control points position as geometrical

parameters (i.e. $G = d\mathcal{N}_g$ and $[\boldsymbol{P}_i(\boldsymbol{\mu})]_j = \boldsymbol{\mu}_{(i-1)d+j}$, $i = 1, \ldots, \mathcal{N}_g$, $j = 1, \ldots, d$) results in an extremely high parameter space dimension $G \gg 1$ which, in turn, may lead to poor performance of the reduced order model [e.g. due to an intractable number of terms in the affine expansions (12)]. The aim of this section is to introduce an efficient representation of the deformation of parametrized domains described by the IGA transformation (4).

Free-form deformation map

Free-form deformation (FFD) techniques, introduced in [43] in the late 80s, are a powerful tool for the deformation of a computational domain by means of a small number of displacements. FFD maps have been employed in the reduced order modelling framework for the first time in [54], as well as applied to shape optimization problems in [55], in both cases considering an underlying finite element high-fidelity discretization. FFD has been exploited in [54,55] to handle the deformation of $\overline{\Omega}$ into $\Omega(\boldsymbol{\mu})$ as the result of the application of the FFD map to each node of the finite element mesh. In contrast, in this work, we apply FFD to *IGA control points* to obtain their deformed position $\{\boldsymbol{P}_i(\boldsymbol{\mu})\}_{i=1}^{\mathcal{N}_g}$, and then rely on the map $\boldsymbol{c}(\mathbf{s}; \cdot)$ in (4) to describe the deformed domain $\Omega(\boldsymbol{\mu})$. To further highlight the sequential nature between the high-fidelity IGA spatial description and the application of FFD map to its control points we will follow the original derivation in [43], that uses a different set of basis functions (Bernstein polynomials) than the more general ones employed in "Problem formulation and isogeometric analysis-based high-fidelity approximation" section. In any case, further extensions to B-splines or NURBS can also be pursued [56].

Denote by $D \subset \mathbb{R}^d$ a box that contains all IGA control points $\{\boldsymbol{P}_i(\boldsymbol{0})\}_{i=1}^{\mathcal{N}_g}$ obtained (e.g.) for $\boldsymbol{\mu} = \boldsymbol{0}$. Moreover, in order to apply Bernstein polynomials defined on the reference hypercube[2] $\overline{D} = [0, 1]^d$, let $\boldsymbol{\psi}(\boldsymbol{p})$ be the affine function that maps D to $\overline{D}$. A (second) set of equispaced control points $\{\boldsymbol{Q}_j\}_{j=1}^{N_g}$, namely the *FFD control points* is introduced, where $N_g := \prod_{k=1}^d N_{g,k}$ being $N_{g,k}$ the number of FFD control points in the coordinate direction k. The deformed position of the j-th control point is then obtained as $\boldsymbol{Q}_j + \boldsymbol{\mu}_j$. Since it is possible for some FFD control points to be fixed or to be allowed to move only in some prescribed coordinate direction, the parameter vector $\boldsymbol{\mu} \in \mathbb{R}^G$ will contain only the non-zero displacement components, so that $G \le dN_g$. Effective computational reduction is obtained if $N_g \ll \mathcal{N}_g$; numerical tests will show that only a small number of FFD control points will be necessary to obtain a large range of admissible shapes.

The *Free-Form Deformation* map $\boldsymbol{T}(\cdot; \boldsymbol{\mu}) : D \to \mathbb{R}^d$ is defined as the composition

$$\boldsymbol{T}(\boldsymbol{p}; \boldsymbol{\mu}) = \boldsymbol{\psi}^{-1}(\overline{\boldsymbol{T}}(\boldsymbol{\psi}(\boldsymbol{p}); \boldsymbol{\mu})),$$

where $\overline{\boldsymbol{T}}(\cdot; \boldsymbol{\mu}) : \overline{D} \to \mathbb{R}^d$ is

$$\overline{\boldsymbol{T}}(\overline{\boldsymbol{p}}; \boldsymbol{\mu}) = \sum_{j=1}^{N_g} \boldsymbol{b}_j(\overline{\boldsymbol{p}}) \, [\boldsymbol{Q}_j + \boldsymbol{\mu}_j], \tag{13}$$

and $\boldsymbol{b}_j(\overline{\boldsymbol{p}})$ is the tensor product of one-dimensional Bernstein polynomials

$$\boldsymbol{b}_j(\overline{\boldsymbol{p}}) = b_{j_1}(\overline{p}_1) \ldots b_{j_d}(\overline{p}_d), \qquad b_{j_k}(\overline{p}_k) = \binom{N_k}{j_k}(1 - \overline{p}_{j_k})^{N_{g,k} - j_k} \, \overline{p}_k^{j_k}.$$

---

[2]Even though actually $\overline{D} = \overline{\Omega}$, we use different symbols to stress the fact that the two reference domains can be, in principle, different depending on the choice of IGA and FFD basis functions.

Salmoiraghi *et al. Adv. Model. and Simul. in Eng. Sci.*(2016)3:21

Page 8 of 22

Finally, the parametrized position of each IGA control point is obtained applying the FFD as follows:

$$\boldsymbol{P}_i(\boldsymbol{\mu}) = \boldsymbol{T}(\boldsymbol{P}_i(\boldsymbol{0}); \boldsymbol{\mu}).$$

More practical geometrical parameters in channel configurations

One of the drawbacks of FFD from practical point of view is the lack of immediate interpretation of its parameters. Indeed, FFD is not interpolatory, so the magnitude of the displacement of a control point is not exactly equal to the actual deformation obtained at that spatial location. Recent works have improved the versatility (from the user point of view) of complex shape parametrization techniques thanks to the automatic prescription of control points position based on more intuitive geometrical parameters [57,58]. In particular, for the test cases of "High-fidelity IGA solver validation" and "Reduced order approximation of Poiseuille-like ows with meanline FFD" sections, we take advantage of similiar ideas to propose a *meanline FFD* based on two (and four) intuitive geometrical parameters related to two (and four) admissible rotations of the meanline of a channel configuration. For the case of two rotations, a summary of the meanline FFD is shown in Fig. 2. For the four rotation case, the extension is straightforward. Starting from a reference mesh Ω and associated IGA control points $\left\{\boldsymbol{P}_i(\boldsymbol{0})\right\}_{i=1}^{\mathcal{N}_g}$ (Fig. 2a), a bounding box D and a lattice of FFD control points $\{\boldsymbol{Q}_j\}_{j=1}^{N_g}$ are introduced (Fig. 2b). The reference meanline of D is divided in four intervals (Fig. 2c). In particular, in view of obtaining different channel configurations, we employ two *intuitive geometrical parameters* θ_1 and θ_2 related to the rotation of the second and third interval (Fig. 2d). FFD geometrical parameters $\{\boldsymbol{\mu}_j\}_{j=1}^{N_g}$ are then *automatically* updated, being zero for all FFD control points in the first and last section, and rotated by θ_1 (θ_2, respectively) in the second (third, respectively) section, as shown in Fig. 2e. Finally, the position of IGA control points $\left\{\boldsymbol{P}_i(\boldsymbol{\mu})\right\}_{i=1}^{\mathcal{N}_g}$ is updated and (4) is applied to get the deformed domain $\Omega(\boldsymbol{\mu})$ (see Fig. 2f). Since the relation between (θ_1, θ_2) and the FFD parameters $\{\boldsymbol{\mu}_j\}_{j=1}^{N_g}$ can be automatically obtained in "High-fidelity IGA solver validation" and "Reduced order approximation of Poiseuille-like ows with meanline FFD" sections we will refer to the former as geometrical parameters. Nevertheless, for the sake of exposition in the next section we still maintain the more general notation $\boldsymbol{\mu}$ to denote them.
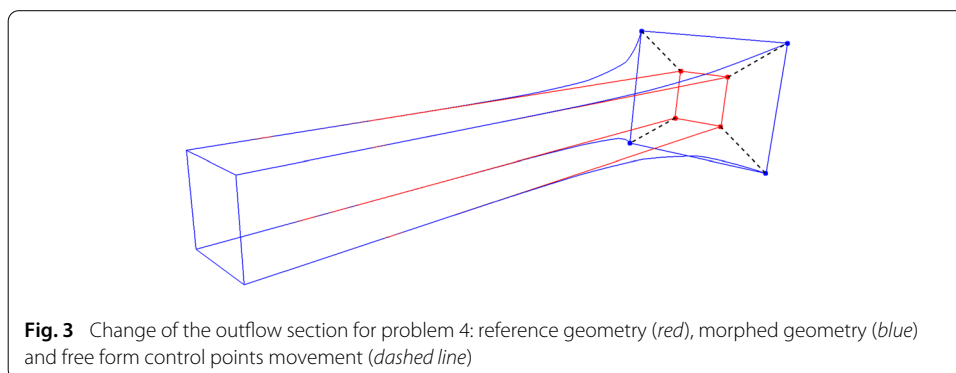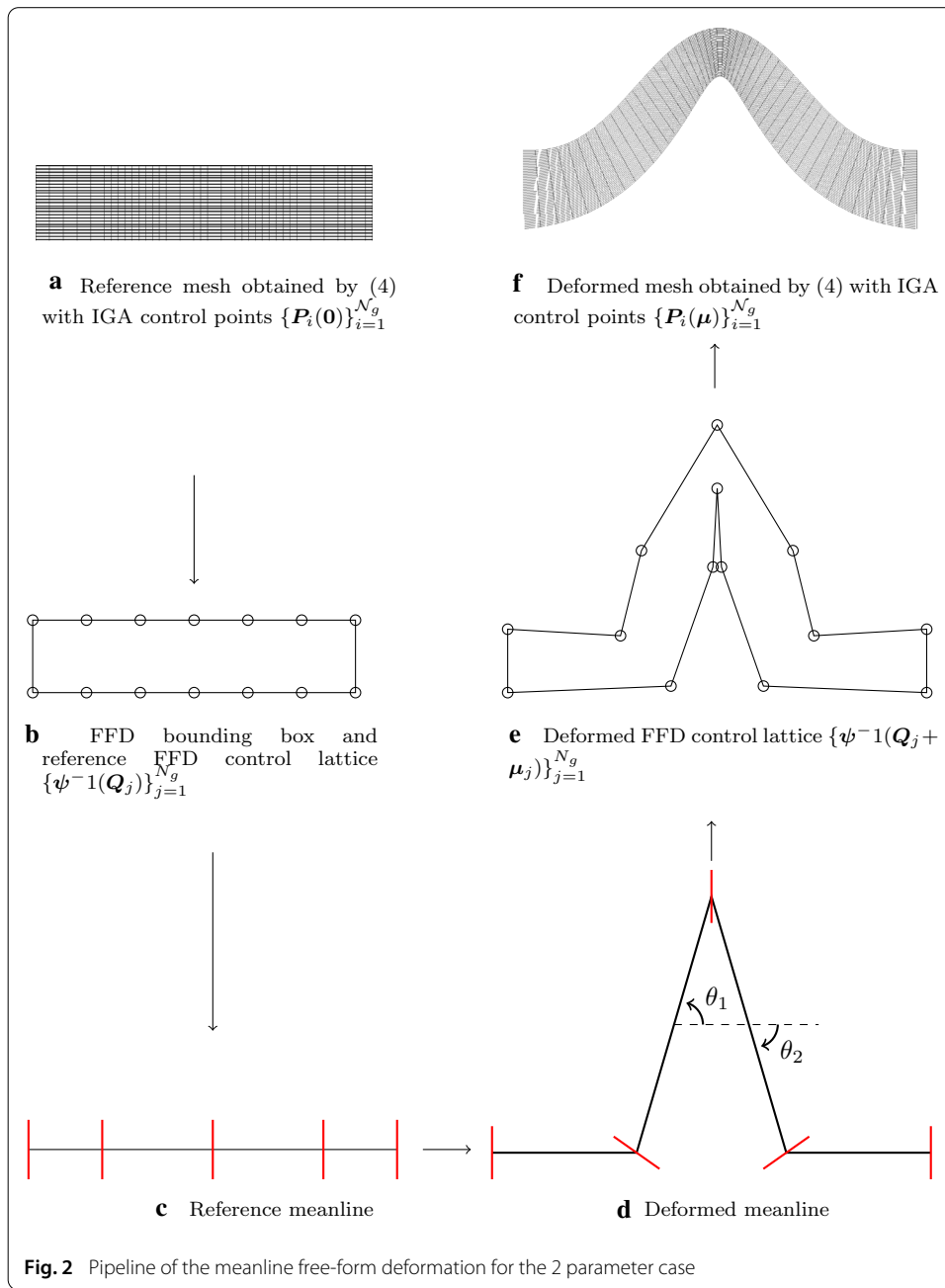
In a similar way, FFD can also be employed to perform local variations to the section area. In particular, FFD is applied in Fig. 3 to enlarge the outlet section of 3D channel with rectangular section. This requires one geometrical parameter in 2D (related to the height of the outlet section) and two geometrical parameters in 3D (related to the width and height of the outlet section).

A POD-Galerkin ROM for parametrized Stokes equations

In this section we summarize a reduced order model (ROM) for parametrized Stokes equations based on a POD method and a Galerkin projection (see [59] for a deeper insight in the subject).

Reduced basis construction through Proper Orthogonal Decomposition

In the offline stage, denote by $\Xi_{\text{train}} = \{\boldsymbol{\mu}^1, \dots, \boldsymbol{\mu}^{N_{\text{train}}}\} \subset \mathcal{D}$ a (usually large) training set of N_{train} points. For each sample point $\boldsymbol{\mu}^i$ the high-fidelity IGA solver is queried to obtain truth velocity and pressure solution. The following snapshot matrices are then considered

Salmoiraghi *et al. Adv. Model. and Simul. in Eng. Sci.*(2016)3:21

Page 9 of 22

a Reference mesh obtained by (4) with IGA control points $\{P_i(0)\}_{i=1}^{\mathcal{N}_g}$

f Deformed mesh obtained by (4) with IGA control points $\{P_i(\mu)\}_{i=1}^{\mathcal{N}_g}$

b FFD bounding box and reference FFD control lattice $\{\psi^-1(Q_j)\}_{j=1}^{N_g}$

e Deformed FFD control lattice $\{\psi^-1(Q_j + \mu_j)\}_{j=1}^{N_g}$

c Reference meanline

d Deformed meanline

Fig. 2 Pipeline of the meanline free-form deformation for the 2 parameter case

Fig. 3 Change of the outflow section for problem 4: reference geometry (*red*), morphed geometry (*blue*) and free form control points movement (*dashed line*)

Salmoiraghi *et al. Adv. Model. and Simul. in Eng. Sci.*(2016)3:21

Page 10 of 22

$$\underline{\mathbf{S_u}} = [\underline{\mathbf{u}}(\mu^1) \mid \ldots \mid \underline{\mathbf{u}}(\mu^{N_{\text{train}}})] \in \mathbb{R}^{\mathcal{N}_u \times N_{\text{train}}},$$

$$\underline{\mathbf{S}}_p = [\underline{\mathbf{p}}(\mu^1) \mid \ldots \mid \underline{\mathbf{p}}(\mu^{N_{\text{train}}})] \in \mathbb{R}^{\mathcal{N}_p \times N_{\text{train}}}.$$

A POD basis for the velocity and pressure reduced spaces are then obtained by a thin singular value decomposition (SVD) of the snapshot matrices, i.e.

$$\underline{\mathbf{X}}_{\mathbf{u}}^{1/2}\underline{\mathbf{S_u}} = \underline{\mathbf{U_u}}\underline{\mathbf{6_u}}\underline{\mathbf{W_u}}^T, \qquad \underline{\mathbf{X}}_p^{1/2}\underline{\mathbf{S}}_p = \underline{\mathbf{U}}_p\underline{\mathbf{6}}_p\underline{\mathbf{W}}_p^T$$

where

- $\underline{\mathbf{X_u}} \in \mathbb{R}^{\mathcal{N}_{\mathbf{u}} \times \mathcal{N}_{\mathbf{u}}}$ ($\underline{\mathbf{X}}_p \in \mathbb{R}^{\mathcal{N}_p \times \mathcal{N}_p}$, respectively) is the matrix representing the velocity (pressure, respectively) inner product;
- $\underline{\mathbf{U_u}} \in \mathbb{R}^{\mathcal{N}_{\mathbf{u}} \times N_{\text{train}}}$ ($\underline{\mathbf{U}}_p \in \mathbb{R}^{\mathcal{N}_p \times N_{\text{train}}}$, respectively) contains the velocity (pressure, respectively) left singular vectors of $\underline{\mathbf{S_u}}$ ($\underline{\mathbf{S}}_p$, respectively);
- $\underline{\mathbf{W_u}} \in \mathbb{R}^{N_{\text{train}} \times N_{\text{train}}}$ ($\underline{\mathbf{W}}_p \in \mathbb{R}^{N_{\text{train}} \times N_{\text{train}}}$, respectively) is an orthogonal matrices of the velocity (pressure, respectively) right singular vectors of $\underline{\mathbf{S_u}}$ ($\underline{\mathbf{S}}_p$, respectively);
- $\underline{\mathbf{6_u}} \in \mathbb{R}^{N_{\text{train}} \times N_{\text{train}}}$ ($\underline{\mathbf{6}}_p \in \mathbb{R}^{N_{\text{train}} \times N_{\text{train}}}$, respectively) is a diagonal matrix, containing the *singular values* of $\underline{\mathbf{S_u}}$ ($\underline{\mathbf{S}}_p$, respectively) sorted in descending order.

Moreover, the so-called *supremizer enrichment* is employed in this work in order to satisfy the inf-sup stability also at the reduced order level [59–61]. Thus, for each training sample the following elliptic problem is solved

$$\underline{\mathbf{X_u}}\underline{\mathbf{s}}(\mu^i) = \underline{\mathbf{B}}^T(\mu^i)\underline{\mathbf{p}}(\mu^i), \quad i = 1, \ldots, N_{\text{train}}.$$

The resulting supremizer snapshots $\underline{\mathbf{s}}(\mu^i)$, $i = 1, \ldots, N_{\text{train}}$ are then stored in a snapshot matrix $\underline{\mathbf{S_s}}$, on which a thin SVD is performed as described previously.

Finally, the reduced spaces dimensions $N_{\mathbf{u}}$ are chosen such that the retained energy $I_{\mathbf{u}}$, given by the sum of the squares of the singular values up to $N_{\mathbf{u}}$ normalized by the sum up to N_{train}, is larger than a prescribed treshold. A similar procedure is applied to choose $N_{\mathbf{s}}$ and N_p. The basis functions of the reduced velocity space V_N are then obtained as the union of the first $N_{\mathbf{u}}$ left singular vectors of $\underline{\mathbf{X}}_{\mathbf{u}}^{1/2}\underline{\mathbf{S_u}}$ to the first $N_{\mathbf{s}}$ left singular vectors of $\underline{\mathbf{X}}_{\mathbf{u}}^{1/2}\underline{\mathbf{S_s}}$. Similarly, the basis functions of the reduced pressure space Q_N are given by the first N_p left singular vectors of $\underline{\mathbf{X}}_p^{1/2}\underline{\mathbf{S}}_p$. The corresponding basis function matrices, that hold the basis functions as column vectors, are denoted by $\mathcal{Z}_{\mathbf{u,s}}$ and $\mathcal{Z}_p$, respectively.

Reduced order approximation through Galerkin projection on the reduced spaces

In the online stage, we let $\mu \in \mathcal{D}$ be a new value and we seek an approximation of the form

$$\underline{\mathbf{u}}(\mu) \approx \mathcal{Z}_{\mathbf{u,s}}\underline{\mathbf{u}}_N(\mu), \qquad \underline{\mathbf{p}}(\mu) \approx \mathcal{Z}_p\underline{\mathbf{p}}_N(\mu)$$

through a Galerkin projection over the reduced spaces V_N and Q_N. Therefore, the following problem has to be solved:

$$\begin{bmatrix} \underline{\mathbf{K}}_N(\mu) & \underline{\mathbf{B}}_N^T(\mu) \\ \underline{\mathbf{B}}_N(\mu) & \mathbf{0} \end{bmatrix} \begin{Bmatrix} \underline{\mathbf{u}}_N(\mu) \\ \underline{\mathbf{p}}_N(\mu) \end{Bmatrix} = \begin{Bmatrix} \underline{\mathbf{f}}_N(\mu) \\ \mathbf{0} \end{Bmatrix}, \tag{14}$$

where (see e.g. [1] for a detailed description)

$$\underline{\mathbf{K}}_N(\mu) = \mathcal{Z}_{\mathbf{u,s}}^T \underline{\mathbf{K}}(\mu) \mathcal{Z}_{\mathbf{u,s}}, \qquad \underline{\mathbf{B}}_N(\mu) = \mathcal{Z}_p^T \underline{\mathbf{B}}(\mu) \mathcal{Z}_{\mathbf{u,s}}, \qquad \underline{\mathbf{f}}_N(\mu) = \mathcal{Z}_{\mathbf{u,s}}^T \underline{\mathbf{f}}(\mu)$$

and we indicate with $\underline{\mathbf{u}}_N(\mu)$ and $\underline{\mathbf{p}}_N(\mu)$ the $\mathbb{R}^{N_{\mathbf{u}}+N_{\mathbf{s}}}$ and $\mathbb{R}^{N_p}$ vectors of coefficients of the reduced order approximation of velocity and pressure fields. Moreover, thanks to the

Salmoiraghi *et al. Adv. Model. and Simul. in Eng. Sci.*(2016)3:21

Page 11 of 22

affine dependence assumption (12), during the online stage each block the ROM linear system (14) can be assembled as

$$\underline{\mathbf{K}}_N(\boldsymbol{\mu}) = \sum_{q=1}^{Q_K} \Theta_q^K(\boldsymbol{\mu})\underline{\mathbf{K}}_N^q, \qquad \underline{\mathbf{B}}_N(\boldsymbol{\mu}) = \sum_{q=1}^{Q_B} \Theta_q^B(\boldsymbol{\mu})\underline{\mathbf{B}}_N^q, \qquad \underline{\mathbf{f}}_N(\boldsymbol{\mu}) = \sum_{q=1}^{Q_f} \Theta_q^f(\boldsymbol{\mu})\underline{\mathbf{f}}_N^q,$$

where the following matrices have been built at the end of the offline stage and stored in memory:

$$\underline{\mathbf{K}}_N^q = \mathcal{Z}_{\mathbf{u},\mathbf{s}}^T \, \underline{\mathbf{K}}^q \, \mathcal{Z}_{\mathbf{u},\mathbf{s}}, \qquad \underline{\mathbf{B}}_N^q = \mathcal{Z}_p^T \, \underline{\mathbf{B}}^q \, \mathcal{Z}_{\mathbf{u},\mathbf{s}}, \qquad \underline{\mathbf{f}}_N^q = \mathcal{Z}_{\mathbf{u},\mathbf{s}}^T \, \underline{\mathbf{f}}^q,$$

resulting in very efficient ($\mathcal{N}$ independent) online queries. We refer to Fig. 4 for a summary of the proposed reduced order model, where the offline stage is shown in red, while the online phase is displayed in green.

Numerical results

High-fidelity IGA solver validation

In order to validate our framework, we first perform some tests on the high-fidelity method for problem with known, exact solution, both for the two dimensional and three dimensional case. The first test is to recover the divergence-free solution:

Fig. 4 Pipeline of the computational reduction paradigm "at large" for the problem at hand [60]
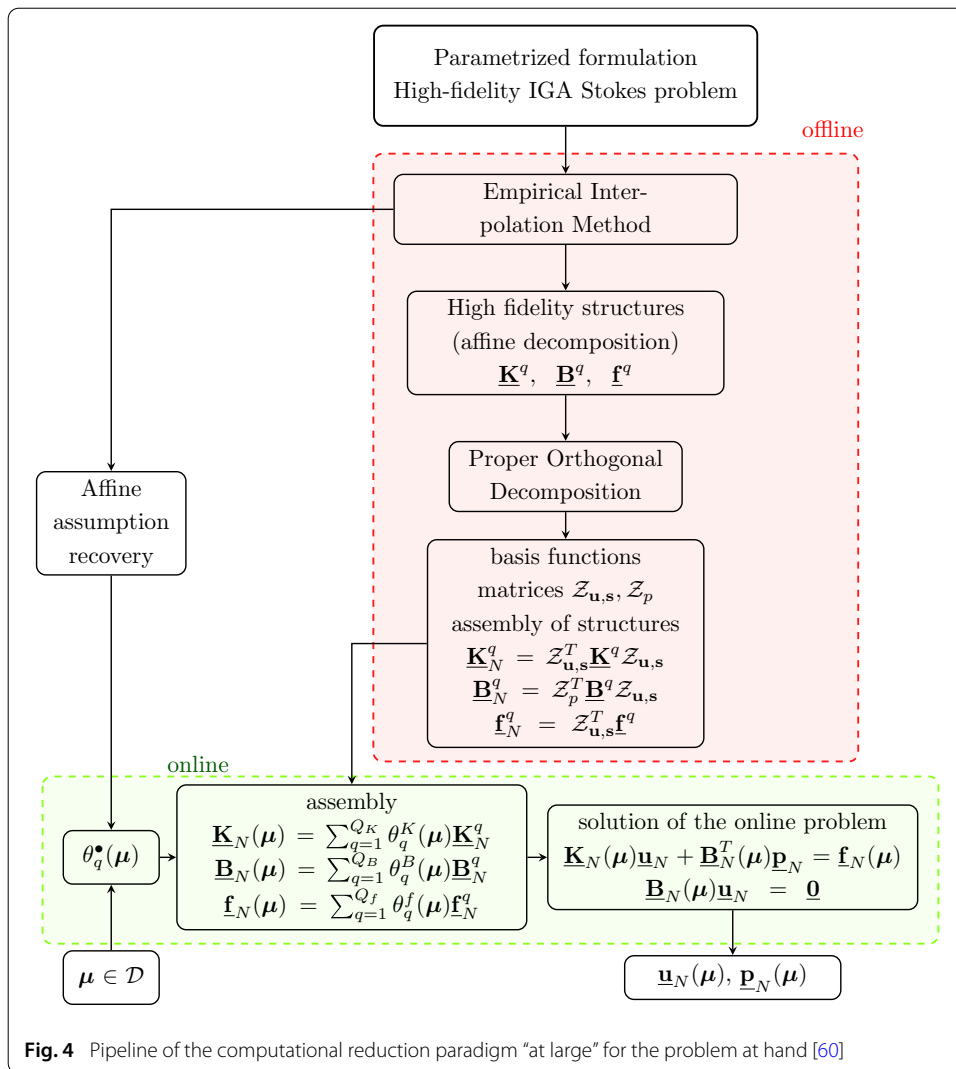
$$\begin{cases} u_x = \pi \cos(\pi x) \cos(\pi y) \\ u_y = \pi \sin(\pi x) \sin(\pi y) \\ u_z = 0 \\ p = \pi^2 \cos(2\pi x) \sin(2\pi y) \end{cases} \quad \text{in } \Omega$$

on a unitary cube $\Omega = [0, 1]^3$. The corresponding forcing term is

$$\begin{cases} f_x = 2\pi^3(\cos(\pi x) \cos(\pi y) - \sin(2\pi x) \sin(2\pi y)) \\ f_y = 2\pi^3(\sin(\pi x) \sin(\pi y) + \cos(2\pi x) \cos(2\pi y)) \quad \text{in } \Omega. \\ f_z = 0 \end{cases} \tag{15}$$

The exact solution is imposed as a Dirichlet boundary condition[3] at $\partial\Omega$.

In Fig. 5 we plot the convergence test for the solution over several refinement cycles on a uniform grid. The rate of convergence is the one predicted by an a priori analysis, as shown in [46]. In Fig. 6 the numerical solution for the last iteration is shown.

As a second test, we consider the two-dimensional Poiseuille flow in a rectangular channel $\Omega = [0, L] \times [-l, l]$ (see Fig. 7), whose solution is analytical:

$$\begin{cases} \boldsymbol{u} = \boldsymbol{u}(y) = (1 - (y/l)^2)\boldsymbol{e}_x \\ p = p(x) \text{ s.t. } \nabla p = -c\boldsymbol{e}_x \\ \boldsymbol{u} = \boldsymbol{u}(0) \quad \text{on } \Gamma_D \\ \boldsymbol{u} = 0 \quad \text{on } \Gamma_W \\ \nu\nabla\boldsymbol{u} \cdot \boldsymbol{n} - p\boldsymbol{n} = 0 \quad \text{on } \Gamma_N \end{cases} \tag{16}$$
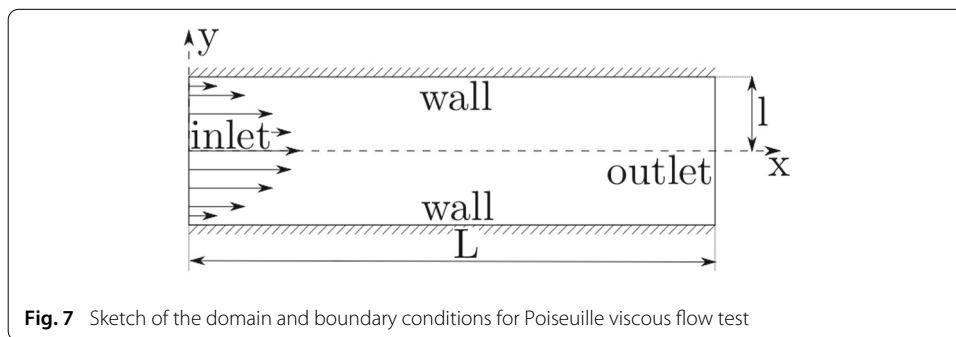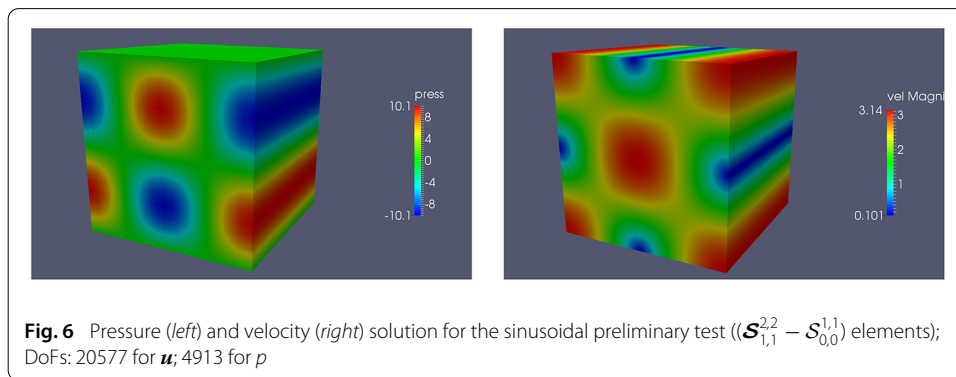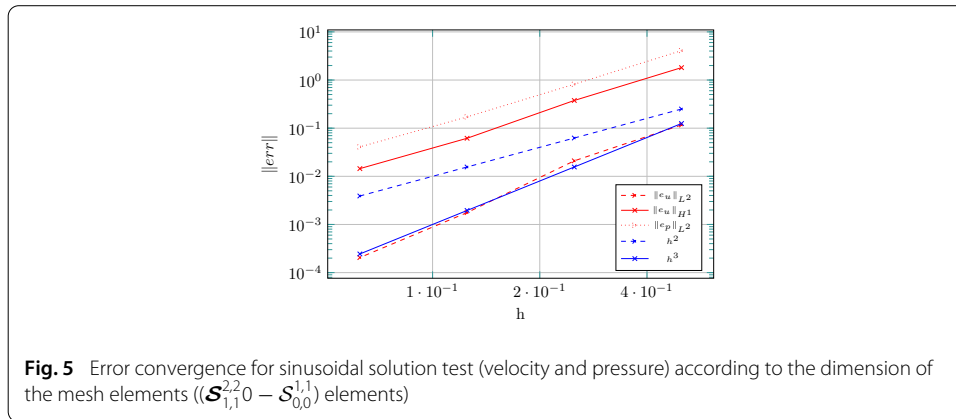
In this case, the error on the numerical solution reaches the machine epsilon already for a single IGA element, that is, for 18 DoFs for $\boldsymbol{u}$ and 4 for p. This behaviour is related to the fact that the solution is quadratic in the velocity and linear in the pressure and the fact that we are using $(\boldsymbol{\mathcal{S}}_{1,1}^{2,2} - \mathcal{S}_{0,0}^{1,1})$ for the solution of the problem for both the preliminary tests. In Fig. 8 we plot the solution for Poiseuille flow on a rectangular domain with $L = 10$ and $l = 0.5$.

Reduced order approximation of Poiseuille-like flows with meanline FFD

Once the code for the Poiseuille flow has been validated, we keep the same model and boundary conditions and deform the original rectangle (for the two dimensional problem) or parallelepiped (for the three dimensional case) domain through FFD, obtaining a family of possible different configuration of Poiseuille-like flows, such as the one depicted in Figs. 9, 10, 21, and provide main results regarding the ROM framework explained in "A POD-Galerkin ROM for parametrized Stokes equations" section.

A summary of the computational details is given in Table 1. In Fig. 11 we provide the geometry of the four problems we treat during the model order reduction: problem 1 characterized by two rotations and 2D $(\boldsymbol{\mathcal{S}}_{1,1}^{2,2} - \mathcal{S}_{0,0}^{1,1})$ elements, problem 2 featuring two rotation problem and an approximation by high-order 2D $(\boldsymbol{\mathcal{S}}_{4,4}^{5,5} - \mathcal{S}_{3,3}^{4,4})$ elements, problem 3 considering four rotation problem and 2D $(\boldsymbol{\mathcal{S}}_{1,1}^{2,2} - \mathcal{S}_{0,0}^{1,1})$ elements, and problem 4 characterized by two rotations, change of the dimensions of the outflow section and 3D $(\boldsymbol{\mathcal{S}}_{1,1,1}^{2,2,2} - \mathcal{S}_{0,0,0}^{1,1,1})$ elements. Thus, two geometrical parameters, namely angles θ_1 and θ_2

---

[3]Since in this case $\Gamma_N = \emptyset$ we take $Q = L_0^2(\Omega) := \{q \in L^2(\Omega) s.t. \int_\Omega q \, ds = 0\}$

Salmoiraghi *et al. Adv. Model. and Simul. in Eng. Sci.*(2016)3:21

Page 13 of 22

Fig. 5 Error convergence for sinusoidal solution test (velocity and pressure) according to the dimension of the mesh elements (($\boldsymbol{\mathcal{S}}_{1,1}^{2,2}0 - \mathcal{S}_{0,0}^{1,1}$) elements)

Fig. 6 Pressure (*left*) and velocity (*right*) solution for the sinusoidal preliminary test (($\boldsymbol{\mathcal{S}}_{1,1}^{2,2} - \mathcal{S}_{0,0}^{1,1}$) elements); DoFs: 20577 for $\boldsymbol{u}$; 4913 for p

Fig. 7 Sketch of the domain and boundary conditions for Poiseuille viscous flow test

of the meanline FFD introduced in "More practical geometrical parameters in channel configurations" section, are considered for problems 1, 2 and 4, with parameter range $\mathcal{D} = [-75\deg, 75\deg]^2$. In a similar way, four geometrical parameters are considered for problem 3, with parameter range $\mathcal{D} = [-45\deg, 45\deg]^4$. Moreover, for problem 4 we also consider variation of the outlet section, that is, $\mathcal{D} = [-45\deg, 45\deg]^2 \times [0, 2]^2$, being $\boldsymbol{\mu} = [\theta_1, \theta_2, \delta\, l_{out}, \delta\, h_{out}] \in \mathcal{D}$ the parameter vector encoding variation of the meanline channel configuration (angles θ_1 and θ_2) and of the outlet area (width $\delta\, l_{out}$ and height $\delta\, h_{out}$ increments with respect to the undeformed configuration).

The offline stage is carried out sampling from a random set $\Xi_{\text{train}} \subset \mathcal{D}$ of cardinality $|\Xi_{\text{train}}| = 500$. This requires the solution of 500 IGA problems and the computation of the SVD of the snapshot matrix (as explained in "Reduced basis construction through proper orthogonal decomposition" section). The resulting singular values are depicted (in
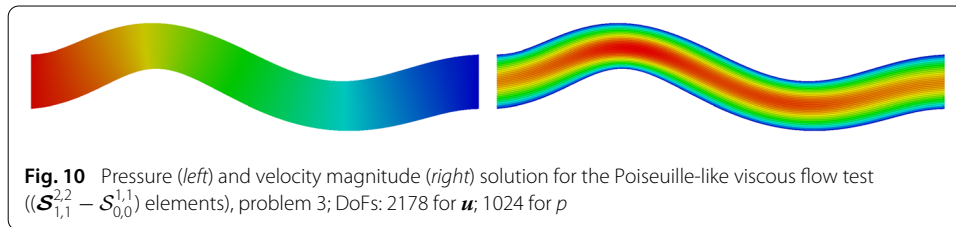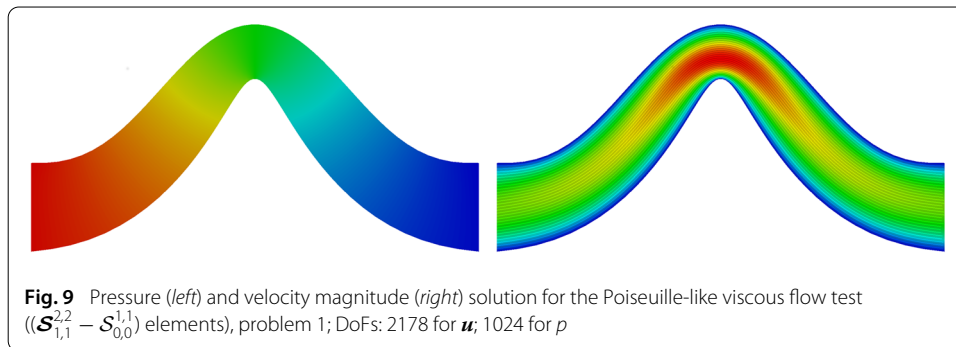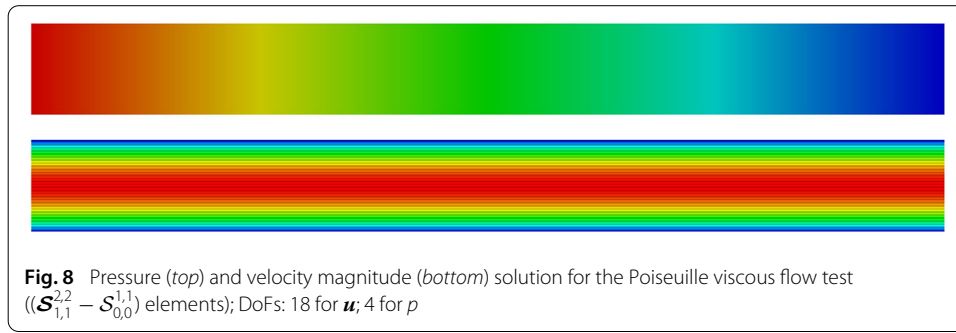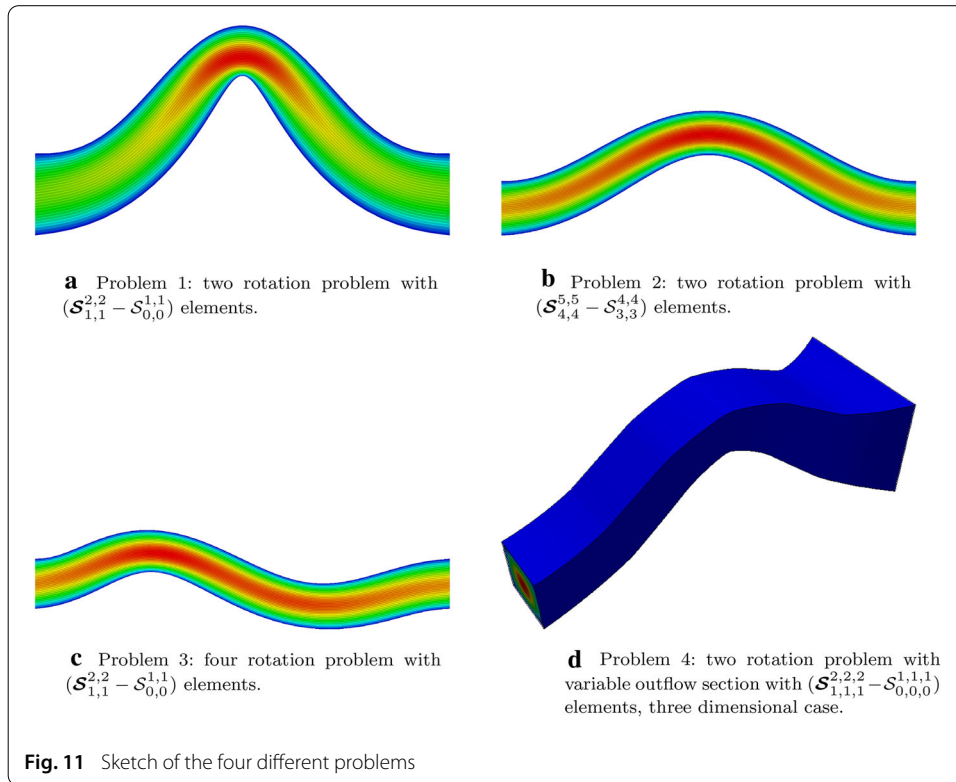
Salmoiraghi *et al. Adv. Model. and Simul. in Eng. Sci.* (2016)3:21

Page 14 of 22

Fig. 8 Pressure (*top*) and velocity magnitude (*bottom*) solution for the Poiseuille viscous flow test $((\boldsymbol{\mathcal{S}}_{1,1}^{2,2} - \mathcal{S}_{0,0}^{1,1})$ elements); DoFs: 18 for $\boldsymbol{u}$; 4 for p

Fig. 9 Pressure (*left*) and velocity magnitude (*right*) solution for the Poiseuille-like viscous flow test $((\boldsymbol{\mathcal{S}}_{1,1}^{2,2} - \mathcal{S}_{0,0}^{1,1})$ elements), problem 1; DoFs: 2178 for $\boldsymbol{u}$; 1024 for p

Fig. 10 Pressure (*left*) and velocity magnitude (*right*) solution for the Poiseuille-like viscous flow test $((\boldsymbol{\mathcal{S}}_{1,1}^{2,2} - \mathcal{S}_{0,0}^{1,1})$ elements), problem 3; DoFs: 2178 for $\boldsymbol{u}$; 1024 for p

Table 1 Computational details about the high-fidelity model and the model order reduction

Problem number	1	2	3	4
Space dimension	2D	2D	2D	3D
IGA space dimension $(\mathcal{N}_v, \mathcal{N}_p)$	(2178, 1024)	(2592, 1225)	(2178, 1024)	(6591, 343)
Number of geometrical parameters	2 rotations	2 rotations	4 rotations	4 = 2 rotations+ outflow variation (length and width)
Geometrical parameters range	$[-75°, 75°]^2$	$[-75°, 75°]^2$	$[-45°, 45°]^4$	$[-75°, 75°]^2 \times [0, 2]^2$
Number of IGA control points	1089	1296	1089	2197
Number of FFD control points	10	10	20	40
EIM tolerance	10^{-3}	10^{-3}	10^{-3}	10^{-3}
EIM terms $Q_K + Q_B + Q_f$	27 + 14 + 0	89 + 22 + 0	50 + 22 + 0	104 + 44 + 0
Number of snapshots	500	500	500	500
POD tolerance $l(N)$	10^{-3}	10^{-2}	10^{-2}	$2 * 10^{-2}$
POD space dimension $(N_{\mathbf{u},\mathbf{s}}, N_p)$	(20, 10)	(20, 10)	(20, 10)	(40, 20)
HF evaluation time	1.5 s	6.1 s	1.5 s	27 s
POD offline construction time	250 s	2344 s	250 s	12325 s
POD evaluation time	0.07 s	0.08 s	0.08 s	0.11 s
Computational speedup POD	20	76	18	245

Salmoiraghi *et al. Adv. Model. and Simul. in Eng. Sci.*(2016)3:21

Page 15 of 22

a Problem 1: two rotation problem with $(\boldsymbol{\mathcal{S}}_{1,1}^{2,2} - \mathcal{S}_{0,0}^{1,1})$ elements.

b Problem 2: two rotation problem with $(\boldsymbol{\mathcal{S}}_{4,4}^{5,5} - \mathcal{S}_{3,3}^{4,4})$ elements.

c Problem 3: four rotation problem with $(\boldsymbol{\mathcal{S}}_{1,1}^{2,2} - \mathcal{S}_{0,0}^{1,1})$ elements.

d Problem 4: two rotation problem with variable outflow section with $(\boldsymbol{\mathcal{S}}_{1,1,1}^{2,2,2} - \mathcal{S}_{0,0,0}^{1,1,1})$ elements, three dimensional case.

Fig. 11 Sketch of the four different problems

decreasing order) in Figs. 12 (Problem 1), 13 (Problem 2), 14 (Problem 3), 15 (Problem 4). The time required for this offline stage ranges from about 250 seconds for problems 1 and 3 to more than 12000 seconds for the three-dimensional problem 4.

In Fig. 16 we perform an error analysis on the solution of the reduced model compared to the high-fidelity one for the geometry configuration of problem 1. In particular, they show that 10 basis functions are enough to have an error lower than 10^{-3} for both pressure and velocity. For the sake of visualization, we also report the reconstructed velocity and pressure fields in Fig. 17 obtained for 10 basis functions. We can compare it with the visualization of the high-fidelity solution of Fig. 9. Similar considerations apply for the other problems: see Fig. 18 for problem 2, Figs. 9, 19 and 20 for problem 3, and Figs. 21, 22 and 23 for problem 4.
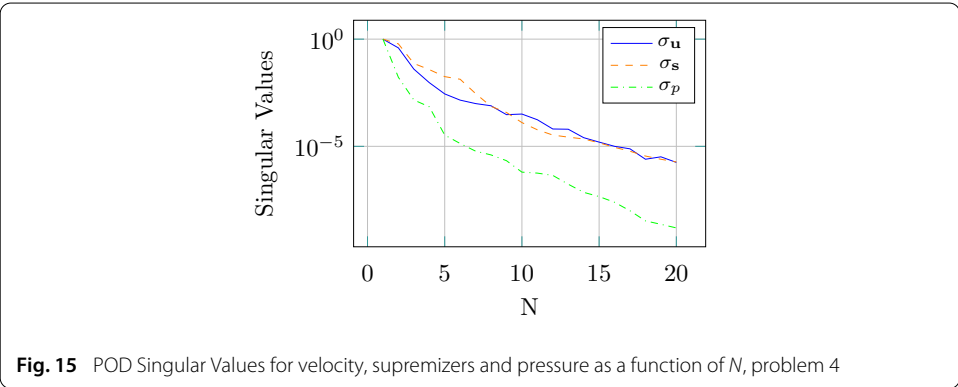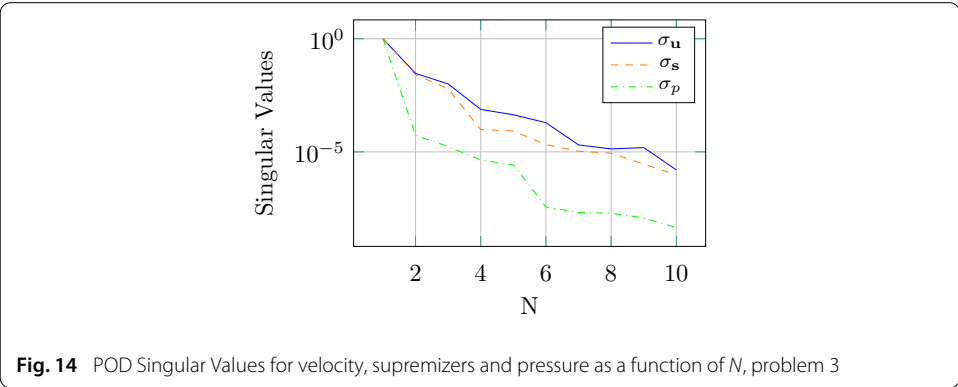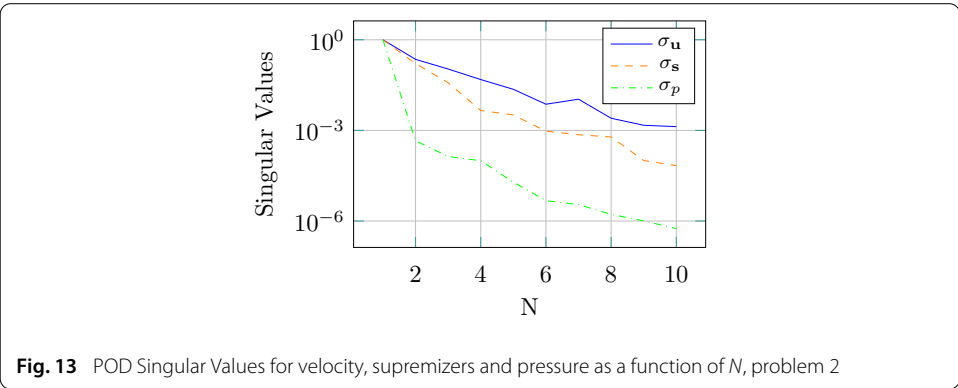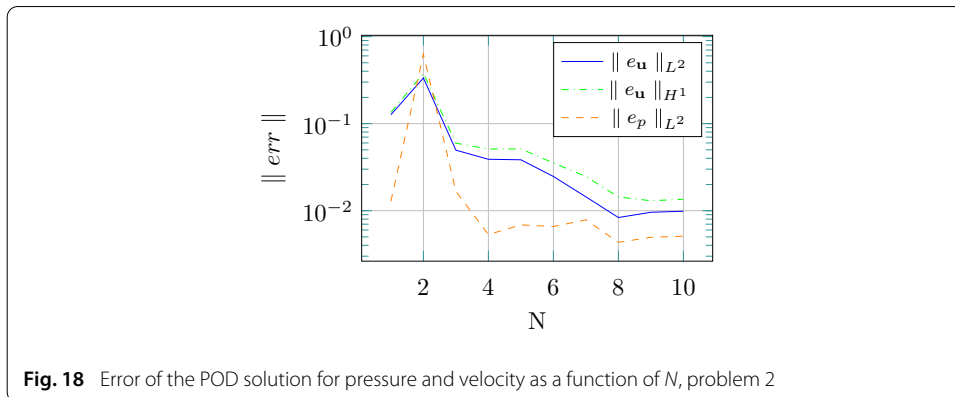

Fig. 12 POD Singular Values for velocity, supremizers and pressure as a function of N, problem 1

Fig. 13 POD Singular Values for velocity, supremizers and pressure as a function of *N*, problem 2

Fig. 14 POD Singular Values for velocity, supremizers and pressure as a function of *N*, problem 3

Fig. 15 POD Singular Values for velocity, supremizers and pressure as a function of *N*, problem 4
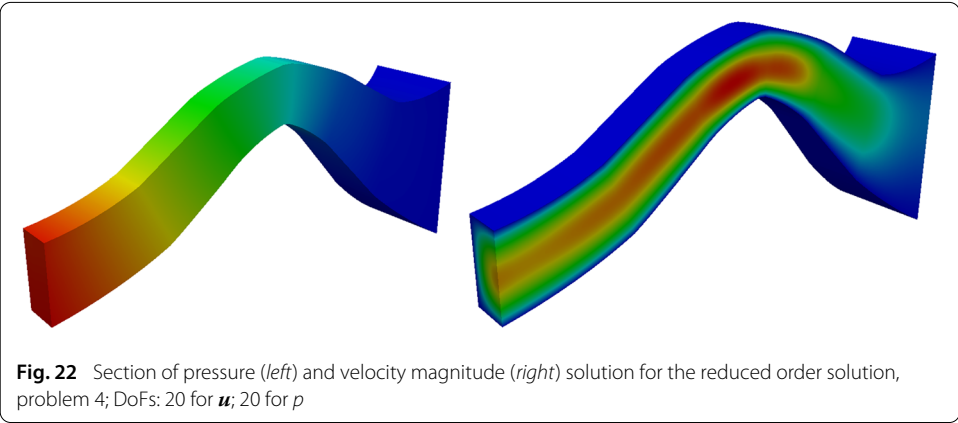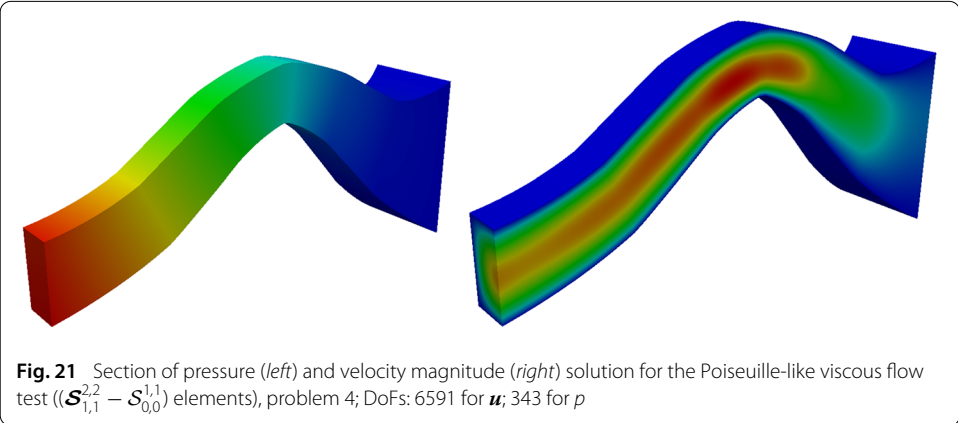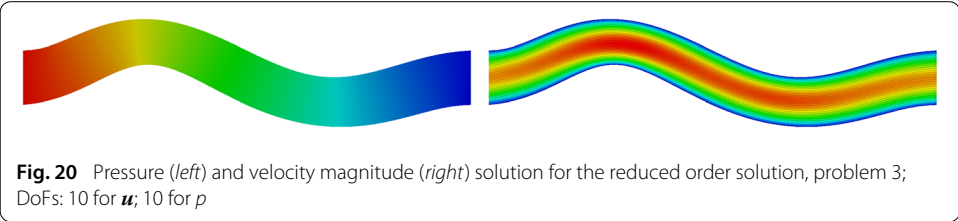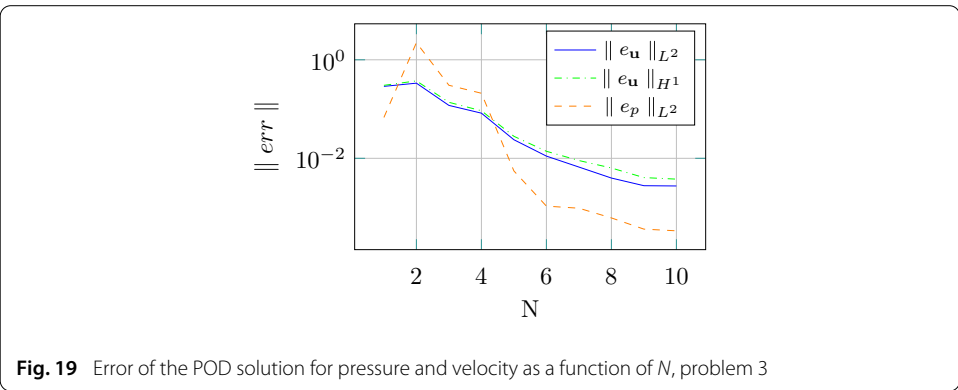
Table 1 also highlights several factors that slightly affect the online performance in terms of CPU time. A first point to take into account is related to the number of terms resulting from the EIM approximation of parametrized tensors: comparing problems 1 to 2 and 3 we can see that both an increased high-fidelity discretization order and an higher number of parameters result in a larger number of EIM terms. A second factor to take into account is related to the reduced space dimension. This can be observed comparing problems 1 and 4, where the latter requires a larger reduced space due to a slower decay of POD singular values. In any case, computational speedups are of at least an order of magnitude. Moreover, problem 4 is characterized by a speedup of order 10^2.

Salmoiraghi *et al. Adv. Model. and Simul. in Eng. Sci.*(2016)3:21

Page 17 of 22

Fig. 16 Error of the POD solution for pressure and velocity as a function of *N*, problem 1

Fig. 17 Pressure (*left*) and velocity magnitude (*right*) solution for the reduced order solution, problem 1; DoFs: 10 for $\boldsymbol{u}$; 10 for p

Fig. 18 Error of the POD solution for pressure and velocity as a function of *N*, problem 2
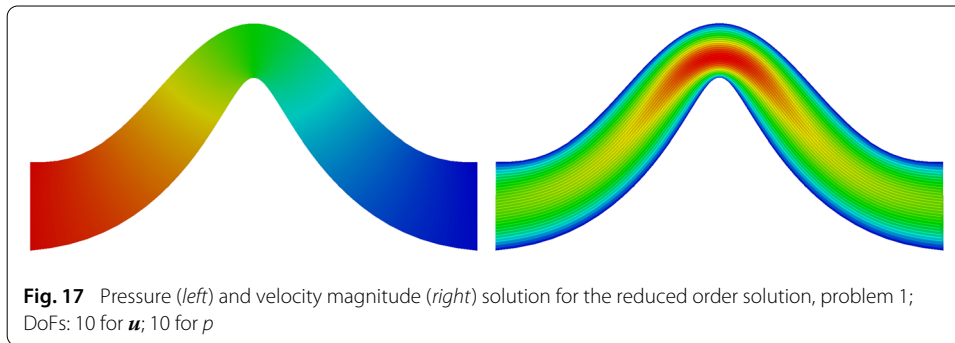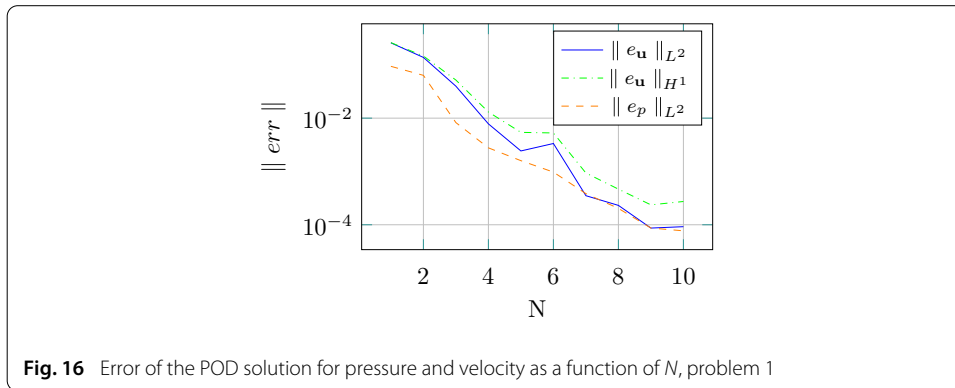
Shape optimization of Poiseuille-like flows with ROM and meanline FFD

We now present the results of the shape optimization routine for the deformable pipe. Motivated by the error analysis of the previous section, we choose $N = 10$. The aim is to find the parameter values that minimize the pressure drop in the pipe, for prescribed inflow section and parametrized meanline variation (and outlet section, in case of problem 4). For prescribed outlet section, the exact result of the optimization procedure is the straight pipe, obtained for null value of the angles; for parametrized outlet section, the exact solution is characterized by null angles and maximum outlet area. The optimal parameter is denoted by $\boldsymbol{\mu}^*$.

Details about the optimization algorithm are summarized in Table 2. In Table 3 we summarize the main results for the optimization process, both for the high fidelity solver and for the reduced order model. The error on the angles and on the pressure drop is negligible in the case of the high fidelity solver. The error for the ROM is of the order
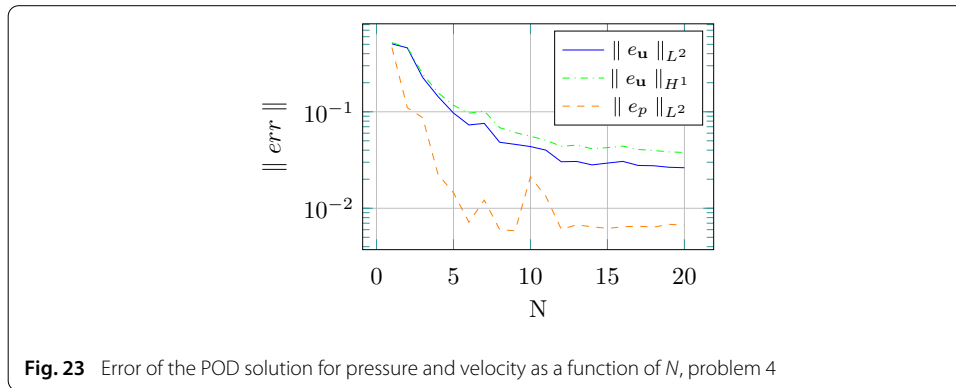
Fig. 19 Error of the POD solution for pressure and velocity as a function of *N*, problem 3

Fig. 20 Pressure (*left*) and velocity magnitude (*right*) solution for the reduced order solution, problem 3; DoFs: 10 for $\boldsymbol{u}$; 10 for p

Fig. 21 Section of pressure (*left*) and velocity magnitude (*right*) solution for the Poiseuille-like viscous flow test (($\boldsymbol{\mathcal{S}}_{1,1}^{2,2} - \mathcal{S}_{0,0}^{1,1}$) elements), problem 4; DoFs: 6591 for $\boldsymbol{u}$; 343 for p

Fig. 22 Section of pressure (*left*) and velocity magnitude (*right*) solution for the reduced order solution, problem 4; DoFs: 20 for $\boldsymbol{u}$; 20 for p

Salmoiraghi *et al. Adv. Model. and Simul. in Eng. Sci.*(2016)3:21

Page 19 of 22

Fig. 23 Error of the POD solution for pressure and velocity as a function of *N*, problem 4

Table 2 Details about the optimization algorithm

Geometrical parameters range	Problem 1	Problem 2	Problem 3	Problem 4
	[−75 deg, 75 deg]		[−45 deg, 45 deg]	[−75 deg, 75 deg]
Optimization algorithm	MATLAB fmincon			
Cost functional J	$\int_{\Gamma_{in}} p\, d\Gamma - \int_{\Gamma_{out}} p\, d\Gamma$			

Table 3 Main results for the optimization process

	Problem 1		Problem 2		Problem 3		Problem 4	
	IGA	**POD**	**IGA**	**POD**	**IGA**	**POD**	**IGA**	**POD**
Opt. CPU time (s)	90	2.5	280	2.5	151	7	1994	5
Opt. speedup	–	36	–	112	–	21	–	400
$\|\boldsymbol{\mu} - \boldsymbol{\mu}^*\|$	10^{-7}	10^{-4}	10^{-5}	10^{-2}	10^{-5}	10^{-3}	10^{-6}	10^{-2}
Pressure drop (J)	80	79.997	80	79.997	80	80.0003	126.43	126.43
Relative error on J	0	$O(10^{-5})$	0	$O(10^{-5})$	0	$O(10^{-6})$	0	$O(10^{-6})$

of 10^{-4} (10^{-4}, respectively), and we obtain a computational speedup of about 36, for the two rotation case. Interestingly, such speedup is considerably higher than the speedup for a single simulation (which is around 20), most likely because it is generally easier for optimization software to explore a smaller state space, and some smarter procedure may be used internally to save computational effort. This behaviour is less evident for the four rotation case (problem 3). We expect that also in the nonlinear case the computational speedup would increase more considerably.

This simple shape optimization test case highlights the capability of the proposed reduced order model (in terms of reducing the computational cost). In future more complex applications will deal with the optimal design process of aero-hydrodynamic components.

Conclusions and future work

We have presented a complete parametric design pipeline from CAD to accurate and efficient numerical simulation, by introducing geometrical parametrization based on FFD, high order simulations based on IGA and efficient and stable computational reduction strategies based on proper orthogonal decomposition, after the enrichment of the velocity space with suited supremizers. This setting is motivated and developed by industrial applications in mechanical, nautical and naval engineering at low Reynolds number (e.g. microfluidics devices characterized by low velocity flows and in small geometrical con-

figurations). Results look promising to continue with the implementation of a viscous non-linear model and more complex physical and geometrical problems in order to deal with more advanced fluid mechanics indexes (vorticity, viscous stresses, viscous energy dissipation), derived from the state equations. For example, we mention the project UBE (Underwater Blue Efficiency) whose goal is the shape optimization of immersed parts of motor yachts, including exhaust flow devices, for the reduction of *emissions* and *vibrations* , in order to increase *on-board comfort*. This parametric design automatic embedded pipeline is motivating also the investigation and improvement of some computational aspects related with FFD and the already mentioned EIM.

Authors' contributions
All authors have prepared the manuscript. All authors read and approved the final manuscript.

Competing interests
The authors declare that they have no competing interests.

References
1.　Hesthaven JS, Rozza G, Stamm B. Certified reduced basis methods for parametrized partial differential equations. SpringerBriefs in mathematics. Berlin: Springer; 2015.
2.　Rozza G, Huynh DBP, Patera AT. Reduced basis approximation and a posteriori error estimation for affinely parametrized elliptic coercive partial differential equations. Arch Comput Methods Eng. 2008;15:1–47.
3.　Christensen EA, Brøns M, Sørensen JN. Evaluation of proper orthogonal decomposition-based decomposition techniques applied to parameter-dependent nonturbulent flows. SIAM J Sci Comput. 1999;21(4):1419–34.
4.　Ravindran SS. A reduced-order approach for optimal control of fluids using proper orthogonal decomposition. Int J Numer Methods Fluids. 2000;34:425–48.
5.　Kunisch K, Volkwein S. Galerkin proper orthogonal decomposition methods for a general equation in fluid dynamics. SIAM J Numer Anal. 2002;40(2):492–515.
6.　Chinesta F, Ladeveze P, Cueto E. A short review on model order reduction based on proper generalized decomposition. Arch Comput Methods Eng. 2011;18(4):395–404.
7.　Chinesta F, Keunings R, Leygue A. The proper generalized decomposition for advanced numerical simulations: a primer. Berlin: Springer; 2013.
8.　Ern A, Perotto S, Veneziani A. Hierarchical model reduction for advection-diffusion-reaction problems. In: Kunisch K, Of G, Steinbach O, editors. Numerical mathematics and advanced applications. Berlin: Springer; 2008. p. 703–10.
9.　Perotto S, Ern A, Veneziani A. Hierarchical local model reduction for elliptic problems: a domain decomposition approach. Mult Model Simul. 2010;8(4):1102–27.
10.　Perotto S, Zilio A. Space-time adaptive hierarchical model reduction for parabolic equations. Adv Model Simul Eng Sci. 2015;2(1):25.
11.　Quarteroni A, Rozza, G. Reduced order methods for modeling and computational reduction. Vol. 9. Berlin: Springer; 2014.
12.　Prud'homme C, Rovas DV, Veroy K, Machiels L, Maday Y, Patera AT, Turinici G. Reliable real-time solution of parametrized partial differential equations: Reduced-basis output bound methods. J Fluids Eng. 2002;124(1):70–80.
13.　Grepl MA, Patera AT. A posteriori error bounds for reduced-basis approximations of parametrized parabolic partial differential equations. ESAIM: M2AN. 2005;39(1):157–81.
14.　Veroy K, Patera A. Certified real-time solution of the parametrized steady incompressible Navier–Stokes equations: rigorous reduced-basis a posteriori error bounds. Int J Numer Methods Fluids. 2005;47(8):773–88.
15.　Quarteroni A, Rozza G, Manzoni A. Certified reduced basis approximation for parametrized partial differential equations and applications. J Math Ind. 2011;1(1):1–49.
16.　Haasdonk B, Ohlberger M. Reduced basis method for finite volume approximations of parametrized linear evolution equations. ESAIM: Math Model Numer Anal. 2008;42(2):277–302.
17.　Ohlberger M, Haasdonk B, Rozza G. A reduced basis method for evolution schemes with parameter-dependent explicit operators. Electron Trans Numer Anal. 2008;32:145–61.
18.　Drohmann M, Haasdonk B, Ohlberger M. Reduced basis approximation for nonlinear parametrized evolution equations based on empirical operator interpolation. SIAM J Sci Comput. 2012;34(2):937–69.
19.　Luo Z, Li H, Sun P, An J, Navon IM. A reduced-order finite volume element formulation based on POD method and numerical simulation for two-dimensional solute transport problems. Math Comput Simul. 2013;89:50–68.
20.　Du J, Zhu J, Luo Z, Navon IM. An optimizing finite difference scheme based on proper orthogonal decomposition for CVD equations. Int J Numer Methods Biomed Eng. 2011;27(1):78–94.

Salmoiraghi *et al. Adv. Model. and Simul. in Eng. Sci.*(2016)3:21

Page 21 of 22

21. Cao Y, Zhu J, Luo Z, Navon IM. Reduced-order modeling of the upper tropical pacific ocean model using proper orthogonal decomposition. Comput Math Appl. 2006;52(8):1373–86.
22. Luo Z, Chen J, Zhu J, Wang R, Navon IM. An optimizing reduced order FDS for the tropical pacific ocean reduced gravity model. Int J Numer Methods Fluids. 2007;55(2):143–61.
23. Kaulmann S, Ohlberger M, Haasdonk B. A new local reduced basis discontinuous Galerkin approach for heterogeneous multiscale problems. Comptes Rendus Mathematique. 2011;349(23):1233–8.
24. Iapichino L. Reduced basis methods for the solution of parametrized PDEs in repetitive and complex networks with application to CFD. PhD thesis, École Polytechnique Fédérale de Lausanne, N. 5529, 2012
25. Antonietti PF, Pacciarini P, Quarteroni A. A discontinuous Galerkin reduced basis element method for elliptic problems. ESAIM: M2AN. 2016;50:337–60.
26. Pacciarini P. Discontinuous Galerkin reduced basis element methods for parametrized partial differential equations in partitioned domains. Ph.D. thesis, Department of Mathematics, Politecnico di Milano, 2016.
27. Roderick O, Anitescu M, Peet Y. Proper orthogonal decompositions in multifidelity uncertainty quantification of complex simulation models. Int J Comput Math. 2014;91(4):748–69.
28. Pitton G, Rozza G. A reduced basis method for bifurcation problems in incompressible fluid dynamics. submitted; 2015.
29. Chahine E, Laborde P, Renard Y. A reduced basis enrichment for the extended finite element method. Math Model Nat Phenom. 2009;4(01):88–105.
30. Niroomandi S, Alfaro I, Gonzalez D, Cueto E, Chinesta F. Real-time simulation of surgery by reduced-order modeling and X-FEM techniques. Int J Numer Methods Biomed Eng. 2012;28(5):574–88.
31. Hughes TJ, Cottrell JA, Bazilevs Y. Isogeometric analysis: cad, finite elements, nurbs, exact geometry and mesh refinement. Comput Methods Appl Mech Eng. 2005;194(39):4135–95.
32. Cottrell JA, Hughes TJ, Bazilevs Y. Isogeometric analysis: toward integration of CAD and FEA. Newyork: Wiley; 2009.
33. Nielsen PN, Gersborg AR, Gravesen J, Pedersen NL. Discretizations in isogeometric analysis of Navier–Stokes flow. Comput Methods Appl Mech Eng. 2011;200(45–46):3242–53. doi:10.1016/j.cma.2011.06.007.
34. Evans JA, Hughes TJ. Isogeometric divergence-conforming b-splines for the steady Navier–Stokes equations. Math Models Methods Appl Sci. 2013;23(08):1421–78.
35. Evans JA, Hughes TJR. Isogeometric divergence-conforming B-splines for the unsteady Navier–Stokes equations. J Comput Phys. 2013;241:141–67. doi:10.1016/j.jcp.2013.01.006.
36. Hosseini BS, Möller M, Turek S. Isogeometric analysis of the Navier–Stokes equations with Taylor–Hood B-spline elements. Appl Math Comput. 2015;267:264–81. doi:10.1016/j.amc.2015.03.104.
37. Wang W, Zhang Y, Liu L, Hughes TJR. Trivariate solid T-spline construction from boundary triangulations with arbitrary genus topology. CAD Comput Aided Des. 2013;45(2):351–60. doi:10.1016/j.cad.2012.10.018.
38. Zhang Y, Bazilevs Y, Goswami S, Bajaj CL, Hughes TJR. Patient-specific vascular NURBS modeling for isogeometric analysis of blood flow. Comput Methods Appl Mech Eng. 2007;196(29–30):2943–59. doi:10.1016/j.cma.2007.02.009.
39. Salmoiraghi F. Reduced order models for potential flows past parametrized NACA airfoils based on an isogeometric boundary element method. Master thesis, Politecnico di Milano. 2014.
40. Manzoni A, Salmoiraghi F, Heltai L. Reduced basis isogeometric methods (RB-IGA) for the real-time simulation of potential flows about parametrized NACA airfoils. Comput Methods Appl Mech Eng. 2015;284:1147–80.
41. Dedè L, Quarteroni A, Zhu S. Isogeometric analysis and proper orthogonal decomposition for parabolic problems. Technical report EPFL MATHICSE 44.2014. 2014.
42. Rinaldi M. Reduced basis method for isogeometric analysis: application to structural problems. Master thesis, Politecnico di Milano. 2014.
43. Sederberg TW, Parry SR. Free-form deformation of solid geometric models. ACM. 1986;20(4):151–60.
44. Aubry N. On the hidden beauty of the proper orthogonal decomposition. Theor Comp Fluid Dyn. 1991;2:339–52.
45. Salmoiraghi F, Ballarin F, Heltai L, Rozza G. Isogeometric analysis based reduced order modelling for incompressible viscous flows in parametrized shapes: applications to underwater shape design. 2015. doi:10.14293/P2199-8442.1. SOP-MATH.P4F56E.v1.
46. Buffa A, De Falco C, Sangalli G. Isogeometric analysis: stable elements for the 2D stokes equation. Int J Numer Methods Fluids. 2011;65(11–12):1407–22.
47. Heltai L, Arroyo M, DeSimone A. Nonsingular isogeometric boundary element method for stokes flows in 3D. Comput Methods Appl Mech Eng. 2014;268:514–39. doi:10.1016/j.cma.2013.09.017.
48. Wang Y, Benson DJ, Nagy AP. A multi-patch nonsingular isogeometric boundary element method using trimmed elements. Comput Mech. 2015. 1–19.
49. Barrault M, Maday Y, Nguyen NC, Patera AT. An empirical interpolation method: application to efficient reduced-basis discretization of partial differential equations. C R Math Acad Sci Paris. 2004;339(9):667–72.
50. Rozza G. Reduced basis methods for Stokes equations in domains with non-affine parameter dependence. Comput Vis Sci. 2009;12(1):23–35. doi:10.1007/s00791-006-0044-7.
51. Quarteroni A, Rozza G. Numerical solution of parametrized Navier-Stokes equations by reduced basis methods. Numer Methods Partial Differ Equ. 2007;23(4):923–48. doi:10.1002/num.20249.
52. Manzoni A, Quarteroni A, Rozza G. Shape optimization for viscous flows by reduced basis methods and free-form deformation. Int J Numer Methods Fluids. 2012;70(5):646–70. doi:10.1002/fld.2712.
53. Lassila T, Quarteroni A, Rozza G. A reduced basis model with parametric coupling for fluid-structure interaction problems. SIAM J Sci Comput. 2012;34(2):1187–213. doi:10.1137/110819950.
54. Lassila T, Rozza G. Parametric free-form shape design with PDE models and reduced basis method. Comput Methods Appl Mech Eng. 2010;199(23–24):1583–92.
55. Ballarin F, Manzoni A, Rozza G, Salsa S. Shape optimization by free-form deformation: existence results and numerical solution for Stokes flows. J Sci Comput. 2014;60(3):537–63.
56. Lamousin HJ, Waggenspack WN Jr. NURBS-based free-form deformations. IEEE Comput Graph Appl. 1994;14(6):59–65.
57. Ballarin F. Reduced-order models for patient-specific haemodynamics of coronary artery bypass grafts. PhD thesis, Department of Mathematics, Politecnico di Milano. 2015. http://hdl.handle.net/10589/102804

58.　Ballarin F, Faggiano E, Ippolito S, Manzoni A, Quarteroni A, Rozza G, Scrofani R. Fast simulations of patient-specific haemodynamics of coronary artery bypass grafts based on a POD–Galerkin method and a vascular shape parametrization. J Comput Phys. 2016;315:609–28.

59.　Ballarin F, Manzoni A, Quarteroni A, Rozza G. Supremizer stabilization of POD-Galerkin approximation of parametrized steady incompressible Navier-Stokes equations. Int J Numer Methods Eng. 2015;102(5):1136–61.

60.　Rozza G, Huynh DBP, Manzoni A. Reduced basis approximation and a posteriori error estimation for Stokes flows in parametrized geometries: roles of the inf-sup stability constants. Numer Math. 2013;125(1):115–52.

61.　Rozza G, Veroy K. On the stability of the reduced basis method for Stokes equations in parametrized domains. Comput Methods Appl Mech Eng. 2007;196(7):1244–60.